EXPERIMENTAL EVALUATION OF CONTACT/IMPACT DYNAMICS BETWEEN A SPACE ROBOT WITH A COMPLIANT WRIST AND A FREE-FLYING OBJECT

N. Uyama, Y. Fujii, K. Nagaoka, and K. Yoshida

Department of Aerospace Engineering, Tohoku University
6-6-01 Aramaki Aza-Aoba, Aoba-ku, Sendai, Miyagi, 980-8579, Japan
uyama@astro.mech.tohoku.ac.jp

ABSTRACT

This paper presents the experimental evaluation of contact/impact dynamics between a space robot with a compliant wrist and a free-flying object. In capturing a target satellite by a free-flying space robot, a robot must prevent bounce-off of a target satellite from the operational space of the robot due to hard collision. In order to avoid hard collision, the authors propose the use of a stiff manipulator equipped with a compliant wrist because this combination is capable of elongating the contact duration with less contact force peak, and hence, makes the contact control possible. In order to understand contact with a compliant wrist, this paper presents the contact dynamics of a uniaxial compliant wrist, which is modeled by a mass-spring-damper system. Then, simplification is presented so that the dominant contact dynamics parameters can be approximated by the stiffness and damping of the compliant wrist. The collision experiment between a manipulator with a compliant wrist and a free-flying target object is conducted using a two-dimensional microgravity emulator, called the air-floating test bed. The contact duration and the coefficient of restitution were chosen as evaluating parameters, and it was verified that both can be expressed by the stiffness and damping of the compliant wrist.

Key words: free-flying space robot, satellite capture, contact dynamics, compliant wrist, coefficient of restitution.

1. INTRODUCTION

In capturing a free-flying satellite in space, there is always possibility that the satellite may bounce off from a space robot, and/or that the satellite may be damaged due to hard collision. In order to avoid such a situation, soft contact utilizing active compliance control and/or passive mechanical compliance is of great interest, especially in autonomous satellite capture operation by a free-flying space robot. For instance, the hybrid force/position controlled, originally proposed by Raibert and Craig[1], and the impedance control, proposed by Hogan[2] are the two major approaches to the introduction of virtual mechanical compliance. However, the active control approach has been facing the difficulty in controlling contact/impact due to the time delay effect because contact/impact is a very short duration phenomenon.

One of the solutions to overcome time delay effect is to increase controllable time by elongating contact duration. This is achieved by introducing passive mechanism, namely mechanical compliance. Mechanical compliance plays an important role to reduce contact force peak and to increase contact duration. However, drawbacks of mechanical compliance are the end tip vibration of a robotic arm and the slow response to control input due to its flexibility.

In order to balance mechanical compliance with fast response, the use of a stiff manipulator with end tip compliance may ideally be suitable. The use of a stiff manipulator makes it possible to obtain fast response, which is suitable for force control. Recent works for satellite capture using a stiff manipulator are, for example, the multiple impedance control by Moosavian and Papadopoulos[3], the impedance control by Yoshida and Nakanishi et al.[4][5]. An example of a passive wrist was created by Salcudean and Hollis, called the IBM magic wrist[6]. Examples of the use of both a stiff manipulator and end tip compliance are the use of passive wrist for contact control by Goswami et al.[7], and brash type of end effector for space debris capture by Nishida et al.[8]. However, force control method in space by a single manipulator with a compliant wrist has not been fully established yet.

In our previous paper, we showed the validity of the use of a stiff manipulator with a compliant wrist to obtain a desired coefficient of restitution by the impedance control with a compliant wrist[9]. In this paper, we concluded that the contact dynamics modeling is inevitable to improve the results of the proposed contact control method.

This paper presents the contact dynamics modeling of a free-flying space robot with a compliant wrist. The contact dynamics model is expressed by a mass-spring-damper system. In order to predict post-contact behavior by a simple algebraic form, the contact dynamics model

is simplified, and the contact dynamics parameters such as stiffness and damping are represented by those of a compliant wrist. In this study, the coefficient of restitution is chosen as an algebraic expression of contact phenomena. The formulae of coefficient of restitution and contact duration are derived from the simplified contact dynamics model. The experimental verification of the proposed contact dynamics model is conducted using a two-dimensional microgravity emulator, called the air-floating test bed. The results of experiment verify the proposed contact dynamics modeling.

2. CONTACT DYNAMICS MODELING OF A UNIAXIAL COMPLIANT WRIST

This section presents the contact dynamics model of a uniaxial compliant wrist. First, the assumptions used in constructing the contact dynamics model are stated. Then, the exact and simplified contact dynamics models are presented.

2.1. Assumptions

In constructing the contact dynamics model of a space robot with a compliant wrist, the following assumptions are introduced.

1. The gravitational acceleration is zero
2. Joints of manipulator are sufficiently stiff.
3. Links of manipulator, a wrist, and a free-flying target object are expressed by a point mass.
4. Point contact is assumed.
5. Contact force is modeled as a continuous spring-dashpot model.
6. A compliant wrist is modeled as a linear mass-spring-damper system.
7. The vibration frequency defined at contact surfaces is sufficiently higher than the one defined at a wrist.
8. The wrist mass is sufficiently smaller than the space robot and the target object.

Based on the above assumptions, the schematic of contact dynamics model for a one-dimensional case is shown in Fig. 1.

2.2. Exact Contact Dynamics Model

The exact contact dynamics model is derived as follows. First, according to the assumption, the contact force can be modeled as a linear spring-dashpot model. Thus, the

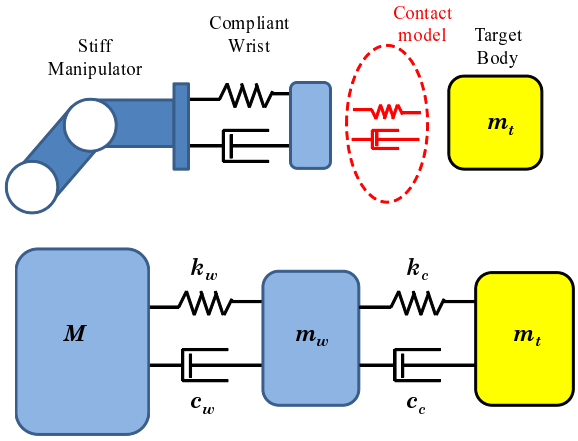

Figure 1. Schematic of a compliant wrist and a free-flying target body, and contact dynamics model.

contact force is expressed in terms of penetration and rate of penetration as follows:

$$\begin{aligned} F_c &= k_c\delta + c_c\dot{\delta} \\ &= k_c(x_t - x_w) + c_c(\dot{x}_t - \dot{x}_w) \end{aligned} \quad (1)$$

where x_t and x_w are the positions of the mass of the target m_t and the compliant wrist m_w, respectively, and k_c and c_c are the stiffness and damping coefficients of actual contact surfaces, respectively. Then, the equations of motion of each mass shown in Fig. 1 are derived as follows:

$$M\ddot{x}_h = -k_w(x_h - x_w) - c_w(\dot{x}_h - \dot{x}_w) \quad (2)$$

$$\begin{aligned} m_w\ddot{x}_w &= -k_w(x_w - x_h) - c_w(\dot{x}_w - \dot{x}_h) \\ &\quad -k_c(x_w - x_t) - c_c(\dot{x}_w - \dot{x}_t) \end{aligned} \quad (3)$$

$$m_t\ddot{x}_t = -k_c(x_t - x_w) - c_c(\dot{x}_t - \dot{x}_w) \quad (4)$$

where M is the equivalent mass projected at the end tip of manipulator; x_h is the position of the end tip of manipulator; and k_w and c_w are the stiffness and damping coefficients of the compliant wrist, respectively.

2.3. Simplified Contact Dynamics Model

In this subsection, a simplified contact dynamics model is presented. A contact dynamics model expressing relative motion before and after contact is necessary to control contact in space. The goal of this contact dynamics modeling is to derive the relationship between pre-contact state and post-contact state of relative motion in the form of the coefficient of restitution, which can be used for contact control. In order to accomplish this goal, the contact dynamics model expressed in Eqs. (2)-(4) is simplified to a single equation of motion.

Suppose that the system expressed in Fig. 1 has no damping, the natural frequency ω of the system is expressed in

the following form.

$$\omega = \left[\frac{1}{2}\left\{\omega_w^2 + \omega_c^2(1+\alpha)\right\} \pm \frac{1}{2}\sqrt{\left\{\omega_w^2 + \omega_c^2(1+\alpha)\right\}^2 - 4\omega_w^2\omega_c^2}\right]^{1/2} \quad (5)$$

$$\omega_w = \sqrt{\frac{k_w}{\tilde{m}_w}}, \quad \omega_c = \sqrt{\frac{k_c}{\tilde{m}_c}}, \quad \alpha = \frac{\tilde{m}_c}{\tilde{m}_w} \quad (6)$$

$$\tilde{m}_w = \frac{Mm_w}{M+m_w}, \quad \tilde{m}_c = \frac{m_w m_t}{m_w+m_t} \quad (7)$$

According to the assumption, the vibration frequency defined at contact surfaces is sufficiently larger than the one defined at a wrist. This condition is expressed as $\omega_w \ll \omega_c$. The wrist mass m_w is also sufficiently smaller than the chaser robot mass M and the target object mass m_t; and hence, the mass ratio α becomes $\alpha \approx 1$.

In an actual system, there exists a damping effect. When the assumption $\omega_w \ll \omega_c$ is satisfied, the vibration between the wrist mass and the target body mass damps out much earlier than the vibration of the wrist itself. Therefore, the dominant natural frequency of the system expressed in Eq. (5) can be approximated as the lowest frequency of the system in the following form.

$$\omega \approx \left[\frac{1}{2}\omega_w^2 + \frac{1}{2}\sqrt{(\omega_w^2)^2}\right]^{1/2} \approx \omega_w \quad (8)$$

$$\omega_w = \sqrt{\frac{k_w}{\tilde{m}}} \quad (9)$$

$$\tilde{m} = \frac{M(m_w+m_t)}{M+m_w+m_t} \quad (10)$$

When the above condition is satisfied, a free-flying target object completely attaches to the end point of wrist and moves together with the wrist mass during contact. This approximation is expressed at the bottom of Fig. 2. In such a case, the equations of motion can be expressed in the following forms.

$$M\ddot{x}_h = -k_w(x_h - x_w) - c_w(\dot{x}_h - \dot{x}_w) \quad (11)$$

$$(m_w+m_t)\ddot{x}_w = k_w(x_h - x_w) + c_w(\dot{x}_h - \dot{x}_w) \quad (12)$$

From Eq. (11) and Eq. (12), a single equation of relative motion is derived as follows.

$$\tilde{m}\ddot{y} = -k_w y - c_w\dot{y} \quad (13)$$

where $y = x_h - x_w$ is the displacement of the compliant wrist.

2.4. Contact Duration and Coefficient of Restitution

This simplification eases the theoretical formulation of contact duration and coefficient of restitution. From Eq. (13), the complete solution with initial conditions $y(0) = 0$ (zero penetration), and $\dot{y}(0) = v_0$ (non-zero rate of penetration), is given by the following:

$$y(t) = \frac{v_0}{\omega_d}e^{-\zeta\omega_w t}\sin\omega_d t \quad (14)$$

where $\omega_d = \sqrt{1-\zeta^2}\omega_w$ is the damped natural frequency, and the ζ is the damping ratio of the system as follows.

$$\zeta = \frac{c_w}{2\sqrt{\tilde{m}k_w}} \quad (15)$$

Eq. (14) expresses the vibration of the compliant wrist. From Eq. (14), the contact duration τ can be derived as the half-period of oscillation ($y(\tau) = 0$) as follows:

$$\tau = \frac{T}{2} = \frac{\pi}{\sqrt{1-\zeta^2}\omega_w} \quad if \;\; 0 \le \zeta < 1 \quad (16)$$

where T is the period of oscillation. For the case $\zeta \ge 1$, the contact duration is theoretically infinity.

$$\tau \to \infty \quad if \quad \zeta \ge 1 \quad (17)$$

Next, the coefficient of restitution ϵ can be expressed in terms of the damping ratio ζ. Using the damping ratio defined in Eq. (15), the time derivative of Eq. (14), and the contact duration given by Eq. (16), the coefficient of restitution ϵ is also expressed as follows:

$$\epsilon = -\frac{\dot{y}(\tau)}{\dot{y}(0)} = e^{-\frac{\zeta\pi}{\sqrt{1-\zeta^2}}} \quad if \;\; 0 \le \zeta < 1 \quad (18)$$

For the case $\zeta \ge 1$, Eq. (18) is no longer valid; instead, the coefficient of restitution becomes zero.

$$\epsilon = 0 \quad if \quad \zeta \ge 1 \quad (19)$$

3. EXPERIMENTAL VERIFICATION

In order to verify the proposed contact dynamics modeling method, the collision experiment between a compliant wrist attached at the tip of a stiff manipulator and a free-flying target object was conducted. The experimental setup is first explained in detail, followed by the experimental conditions. The results and discussion of collision experiment are finally presented.

3.1. Experimental Setup

The experimental setup and its schematic are shown in Figs. 3-4. A microgravity emulation was achieved by the air-floating test bed, which enables an object equipped with air tanks to float on a smooth flat plane with negligibly small friction, utilizing the air bearing principle. The floating target body was equipped with four air pads,

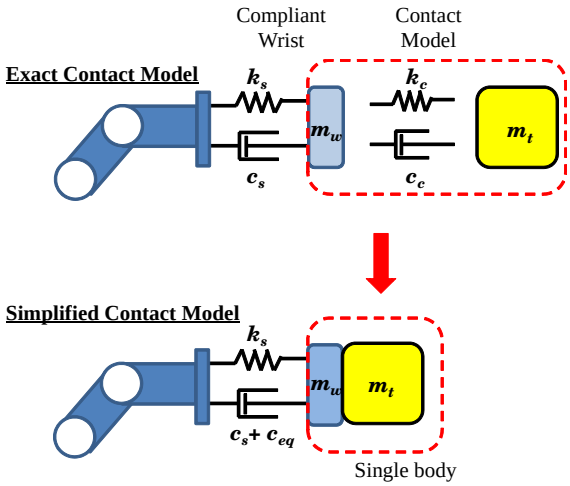

Figure 2. Schematic of exact and simplified contact models.

and each pad was connected to the on-board air tanks by tubes. Each pad floats by static air pressure. The weight of the air-floating body can be changed by adding or subtracting partial weight. Hence, the position of center of mass is adjustable. In this setup, an emulated environment was two-dimensional microgravity plane. The contact point on the air-floating body was designed as a hemisphere so as to realize point contact.

The compliant wrist used in this experiment was a uniaxial compliant wrist, where the motion of the wrist mass was constrained by a linear guide, as shown in Fig. 3(b). The compliant wrist was equipped with a 6-axis force/torque sensor, made by Nitta Corporation, at its end tip of movable part to measure the contact force.

As a space robot model, a ground-based robotic arm, called PA10, made by Mitsubishi Heavy Industry, was used to represent a stiff manipulator. The stiffness of joints of PA10 robotic arm is 10^5 order while the stiffness of the compliant wrist is 10^3 to 10^4 order. Therefore, the vibration of end tip of PA10 robotic arm was assumed to be negligible compared to the one of the compliant wrist.

The motion measurement system used in this experiment was a motion tracking cameras, called OptiTrack. This system uses infrared cameras, each of which tracks the positions of infrared rays reflected from reflective balls attached on the air-floating target body and the compliant wrist.

3.2. Experimental Conditions

This experiment was a one-dimensional collision experiment between the compliant wrist and the floating target body. The contact dynamics parameters are shown in Tab. 1. Since the wrist used in this experiment had friction in its linear guides, the friction effect was estimated

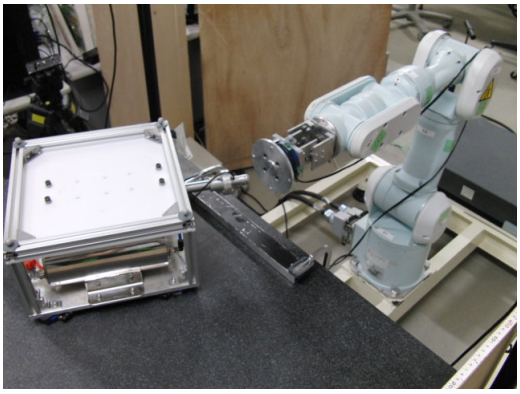

(a) Air-floating test bed and robotic arm PA10

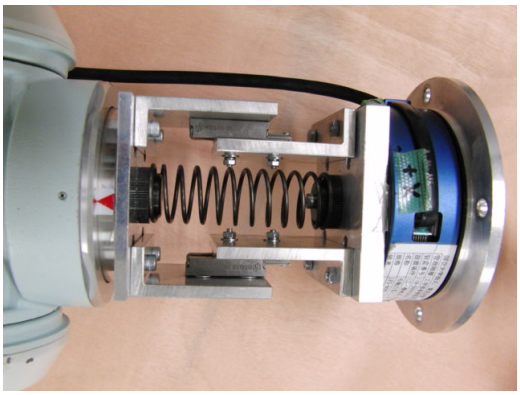

(b) Uniaxial compliant wrist at the tip of PA10

Figure 3. Experimental Setup of Collision Experiment

and included as a form of equivalent viscous damping (c_{eq}), which was approximated as a constant value. For each condition, 5 trials were conducted.

The end tip of PA10 robotic arm was set to an initial position with all servos locked. The air-floating target body was given various initial velocities by hand and collided into the compliant wrist so that the post-contact motion of the air-floating target body did not induce rotation. In this experiment, the position of the center of mass of the air-floating target body was aligned to the direction of contact force so as to minimize the wrench as much as possible.

In this experiment, the contact force and the motion of both the compliant wrist and the air-floating target body were measured. The velocities of the wrist and the target body were computed by taking the time derivative of the position histories. The pre- and post-contact velocities of the air-floating body were computed by taking the average of velocities 1-second before and after contact.

3.3. Experimental Results and Discussion

The resulting coefficient of restitution and contact duration are shown in Fig. 5 and Fig. 6, respectively, where

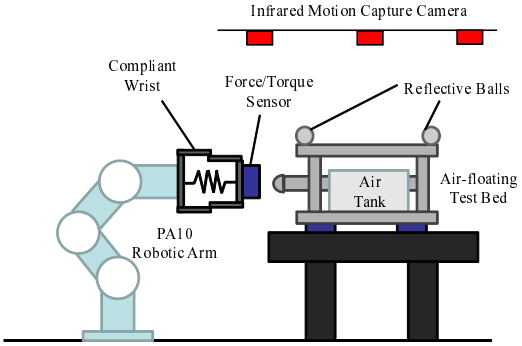

Figure 4. Schematic of Experimental Setup of Collision Experiment.

Table 1. Contact Dynamics Parameters

Name	Variable	Value
Target Mass [kg]	m_t	9.0, 23.2, 35.7, 51.0 63.2
Chaser Mass [kg]	M	huge (10^9)
Wrist Mass [kg]	m_w	0.7
Wrist Stiff. [N/m]	k_w	530, 1020, 3600, 5100
Wrist Damp. [Ns/m]	c_w	1.4, 2.1, 2.8, 2.7
Contact Stiff. [N/m]	k_c	68,000
Contact Damp. [Ns/m]	c_c	unknown
Equiv. Coeff. [Ns/m]	c_{eq}	12.5

dots with error bars are the experimental results, and dashed lines are the theoretical prediction by the simplified contact dynamics model given by Eq. (18). From the graphs, both the resulting coefficient of restitution and contact duration fairly matched the theoretical prediction.

The errors in the coefficient of restitution were mainly due to the model error. In general, the coefficient of restitution is dependent on not only the characteristics of mass, spring and damper, but also the initial colliding velocity, which is not formulated in the proposed linear modeling. The overall average initial colliding velocity was about 7 [cm/s]. In low spring constant cases such as Fig. 5(a) and (b), the average velocity was about 10 [cm/s], which pushed up the resulting coefficient of restitution. Thus, the experiment showed that a velocity-dependent form of coefficient of restitution is needed for further improvement.

Overall, it was concluded that the coefficient of restitution and the contact duration can be predicted with small deviation. One should pay attention to the prediction of the coefficient of restitution when using the proposed linear contact dynamics modeling because of velocity dependency. The improvement in the prediction of the coefficient of restitution may be achieved by appropriately including friction effect.

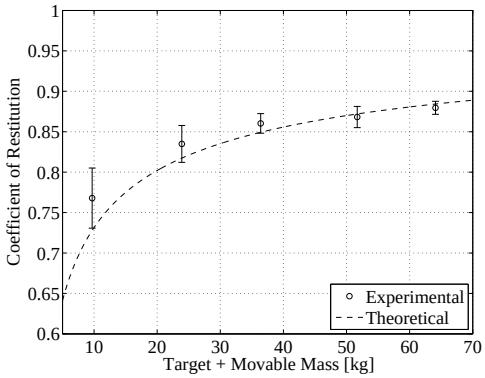

(a) Spring constant k_w = 530 [N/m]

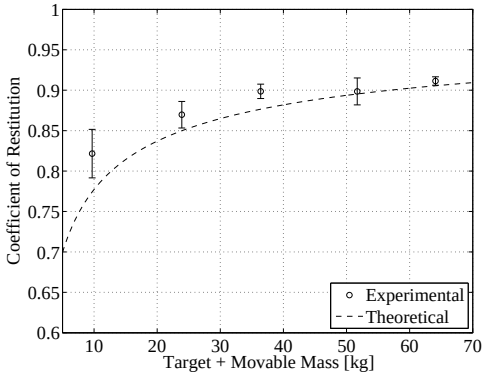

(b) Spring constant k_w = 1,020 [N/m]

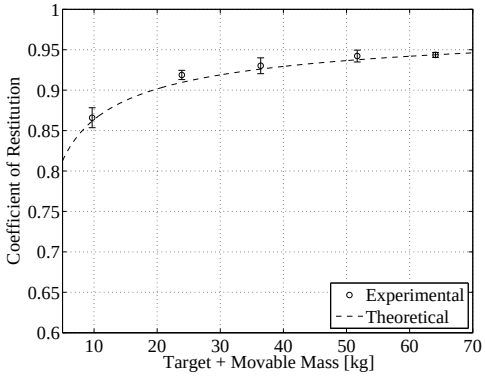

(c) Spring constant k_w = 3,600 [N/m]

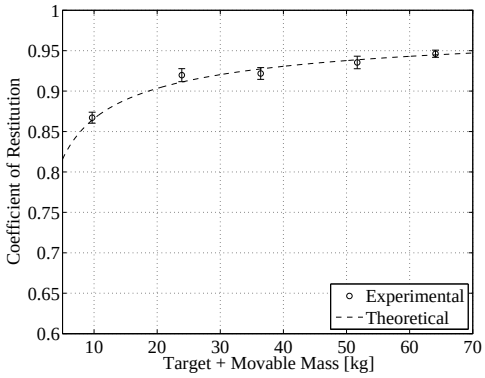

(d) Spring constant k_w = 5,100 [N/m]

Figure 5. Resulting coefficient of restitution vs sum of target mass and movable mass of compliant wrist

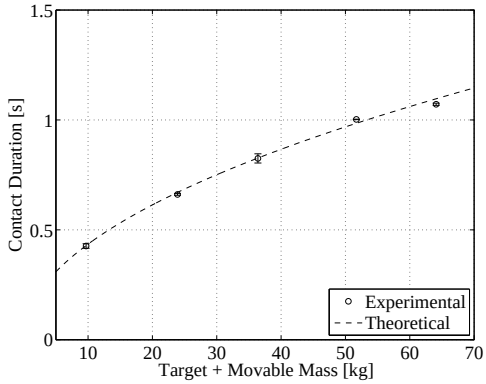

(a) Spring constant k_w = 530 [N/m]

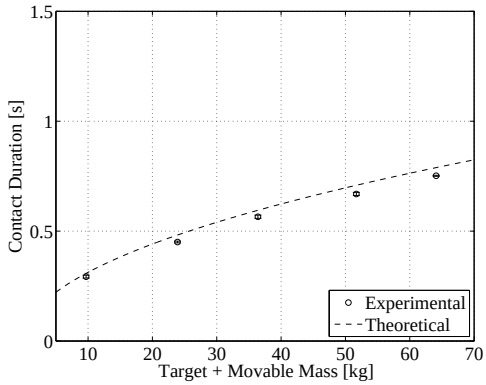

(b) Spring constant k_w = 1,020 [N/m]

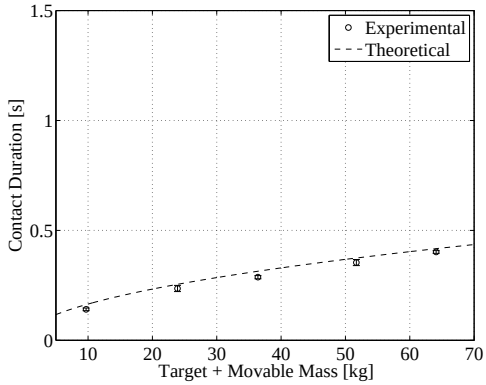

(c) Spring constant k_w = 3,600 [N/m]

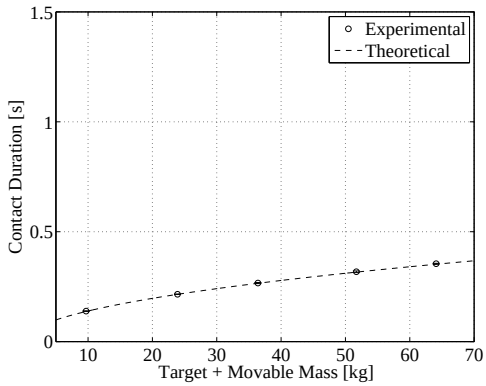

(d) Spring constant k_w = 5,100 [N/m]

Figure 6. Resulting contact duration vs sum of target mass and movable mass of compliant wrist

4. CONCLUSION

This paper presented the contact dynamics modeling of a space robot equipped with a compliant wrist at its end tip. Utilizing a mass-spring-damper model, an exact contact dynamics model of a compliant wrist was formulated. The simplification of contact dynamics model was performed with an assumption that the frequency defined at actual contact surfaces is much higher than the one at a compliant wrist. Using the simplified contact dynamics model, the coefficient of restitution was formulated and became a function of wrist parameters and target mass. The collision experiment was conducted using a two-dimensional microgravity emulator, called the air-floating test bed. The results and discussion of collision experiment verified the proposed contact dynamics modeling of a compliant wrist.

5. ACKOWLEDGMENT

This research was partially supported by Japan Society for the Promotion of Science (JSPS), Grant-in-Aid for JSPS Fellows, No. 22-3505, 2010.

REFERENCES

[1] M. Raibert, J. Craig. (1981). Hybrid Position/Force Control of Manipulators, ASME Journal of Dynamic Systems, Measurement, and Control. Vol. 102. No. 2. pp. 126-133

[2] N. Hogan. (1985). Impedance Control: An Approach to Manipulation: Part 1-3. ASME, Journal of DSMC. pp. 1-7.

[3] S. Ali A. Moosavian. Evangelos Papadopoulos. (1997). On the Control of Space Free-Flyers Using Multiple Impedance Control. Proc. of IEEE Int. Conf. on Robotics and Automation. Albuquerque. New Mexico. pp. 853-858.

[4] K. Yoshida. H. Nakanishi. H. Ueno. N. Inaba. T. Nishimaki. and M. Oda. (2004). Dynamics, control and impedance matching for robotic capture of a non-cooperative satellite. Advanced Robotics. Vol.18. No.2. pp.175-198.

[5] H. Nakanishi. N. Uyama. K. Yoshida. (2010) Virtual Mass of Impedance System for Free-Flying Target Capture. Proc. of IEEE/RSJ Int. Conf. on Intelligent Robots and Systems. Taipei. pp.4101-4106.

[6] S. Salcudean, R. L. Hollis. (1988). A magnetically levitated fine motion wrist: kinematics, dynamics and control. Proc. of 1988 IEEE Int. Conf. on Robotics and Automation. Philadelphia. PA. USA. pp.261-266. Vol. 1.

[7] A. Goswami. M. A. Peshkin. J. E. Colgate. (1990) Passive robotics: an exploration of mechanical computation. Proc. of 1990 IEEE Int. Conf. on Robotics

and Automation. Cincinnati. OH. USA. pp.279-284. Vol. 1.

[8] S. Nishida. S. Kawamoto. (2011) Dynamical Simulations for Space Debris Capture. SICE Annual Conference. Tokyo. Japan. pp. 2283-2286.

[9] N. Uyama. D. Hirano. H. Nakanishi. K. Nagaoka. and K. Yoshida. (2011) Impedance-Based Contact Control of a Free-Flying Space Robot with Respect to Coefficient of Restitution. Proc. of IEEE/SICE Int. Sym. on System Integration. Kyoto. Japan. pp.1196-1201.